CMS Physics Analysis Summary

Contact: cms-pag-conveners-bphysics@cern.ch 2015/12/15

Measurement of the B^+ hadron production cross section in pp collisions at 13 TeV

The CMS Collaboration

Abstract

The B^+ meson differential cross sections, as a function of transverse momentum and rapidity, are measured in pp collisions at center-of-mass energy $\sqrt{s} = 13$ TeV, on the basis of a data sample collected by the CMS experiment, corresponding to an integrated luminosity of 50.8 pb^{-1}. The measurement uses the exclusive decay channel $B^+ \to J/\psi\, K^+$, with the J/ψ decaying to a pair of muons. The results are compared with theory calculations and with measurements made at 7 TeV.

1 Introduction

Measurements of b-hadron production cross sections provide essential information to understand QCD. Such studies have been carried out by several hadron collider experiments, including UA1 [1, 2] at CERN, as well as CDF [3–6] and D0 [7, 8] at Fermilab. The most recent measurements have been performed at the LHC, by CMS [9–12], ATLAS [13, 14], and LHCb [15–17], in pp collisions at center-of-mass energies of $\sqrt{s} = 7$ and/or 8 TeV. Studies of b-hadron production at the higher energies provided by the Run 2 of the LHC provide a new important test of theoretical calculations.

This note describes a measurement of the B^+ differential cross section in pp collisions at 13 TeV, as a function of transverse momentum (p_T^B) and rapidity (y^B). The analysis is based on a data sample collected by the CMS experiment, corresponding to an integrated luminosity of $50.8\,pb^{-1}$, and uses the channel $pp \to B^+X \to J/\psi K^+X$ (charge conjugate states are implied throughout this note), selecting events where the J/ψ decays into a pair of muons.

2 CMS detector and trigger

The central feature of the CMS apparatus is a superconducting solenoid of 6 m internal diameter, providing a magnetic field of 3.8 T. Within the magnet volume are a silicon pixel and strip tracker, a lead tungstate crystal electromagnetic calorimeter, and a brass/scintillator hadron calorimeter. The inner tracker measures charged particles within the pseudorapidity range $|\eta| < 2.5$, where $\eta = -\ln[\tan(\theta/2)]$ and θ is the polar angle with respect to the counterclockwise proton beam direction. Muons are measured with detection planes made using three technologies: drift tubes, cathode strip chambers, and resistive-plate chambers. Matching muons to tracks measured in the silicon tracker results in a p_T resolution better than 1.5% for a typical muon in this analysis. Extensive forward calorimetry complements the angular coverage provided by the barrel and endcap detectors. A more detailed description of the CMS detector can be found in Ref. [18].

The CMS triggers used in this analysis have two levels: the first level (L1) seeds are exclusively based on the information provided by the muon detectors, while the "high level trigger" (HLT) paths also use silicon tracker data to filter the events. Two L1 seeds have been used: one requires two muons in the barrel region ($|\eta^\mu| < 1.6$), without explicitly imposing a minimum p_T value; the other accepts two muons without rapidity restrictions (i.e., $|\eta| < 2.4$) but requires that at least one muon has $p_T > 10$ GeV. The high level trigger requires that the two muons have opposite charge, are within $|\eta| < 2.4$ and have p_T larger than 4 GeV. The dimuon invariant mass, M, must be in the range 2.9–3.3 GeV and the χ^2 probability of the dimuon fit (imposing a common vertex) must be greater than 10%. Furthermore, the trigger purity is enhanced by requiring that the distance between the dimuon vertex and the interaction point is larger than three times its uncertainty, to select dimuons from "non-prompt" J/ψ decays while rejecting almost all the promptly produced J/ψ mesons. Also, the reconstructed J/ψ momentum vector must point back to the interaction point in the transverse plane ($\cos(\alpha) > 0.9$, where α is the angle between J/ψ momentum vector and the vector formed by the interaction point and the dimuon vertex). Finally, the J/ψ candidate is combined with a charged track of $p_T > 0.8$ GeV, and the three-track fit must have normalized χ^2 smaller than 10.

3 Event reconstruction and selection

The first step in the reconstruction of the $B^+ \to J/\psi K^+$ decays is the selection of the events with a pair of muons coming from the decay of the J/ψ mesons. The muons are required to have at least one reconstructed segment in the muon stations that matches the extrapolated position of a track reconstructed in the silicon tracker, $p_T > 4\,\text{GeV}$ and $|\eta| < 2.4$, as well as a good track-fit quality. The muon tracks are required to intersect the beam line within a cylinder of 0.3 cm radius and 20 cm along the beam line, around the interaction point. Candidate J/ψ mesons are reconstructed by combining pairs of oppositely-charged muons having an invariant mass within $\pm 150\,\text{MeV}$ of the nominal J/ψ mass [19]. Each J/ψ candidate must have $p_T > 8\,\text{GeV}$ and the χ^2 probability of the dimuon vertex fit is required to be larger than 10%. Both muons must be within $|\eta| < 1.6$ or one of the muons must have $p_T > 10\,\text{GeV}$.

Candidate B^+ mesons are reconstructed by combining a J/ψ candidate with a charged track of $p_T > 1\,\text{GeV}$. The track is assumed to be a kaon and the track-fit χ^2 must be less than five times the number of degrees of freedom. A kinematic fit is performed to the dimuon-track combination, constraining the dimuon mass to the nominal J/ψ mass. The three-track combination must be compatible with having a common vertex with a vertex-fit χ^2 probability larger than 10% and a reconstructed invariant mass, $M(J/\psi K)$, in the range 5–6 GeV. The transverse decay length significance, defined as the distance between the secondary vertex and the beam spot in the transverse plane, divided by its uncertainty, is required to exceed 3.5. Also, the cosine of the angle between B^+ candidate momentum and the vector formed by the interaction point and the $\mu\mu K$ vertex in the transverse plane must be greater than 0.99.

The combinatorial background resulting from the spurious combination of a promptly produced J/ψ or a J/ψ decayed from a B hadron with an uncorrelated charged particle, is suppressed by placing a requirement on the reconstructed decay length of the B^+ candidate. Given the excellent dimuon mass resolution at the J/ψ mass and the good muon identification performance of the CMS detector, the background level in the J/ψ peak is very small. Additional backgrounds arise from mis-reconstructed b-hadron decays, such as $B \to J/\psi + K + X$ or $B \to J/\psi K^*(892)$, which produce a broad structure in the mass region $M(J/\psi K) < 5.15\,\text{GeV}$.

4 Reconstruction efficiency and acceptance

The detection efficiencies and the geometrical acceptance are jointly evaluated through simulation studies using large samples of B^+ signal generated by PYTHIA 8.205 [20], with the tune CUEP8M1 and decays done by EVTGEN [21], that are processed by the simulation framework of the CMS detector, based on GEANT4 [22]. The efficiency times acceptance is defined as the fraction of $B^+ \to J/\psi K^+ \to \mu^+\mu^- K^+$ decays, generated in the phase space region $10 < p_T^B < 100\,\text{GeV}$ and $|y^B| < 2.4$, that survive the selection criteria. It ranges from $\sim 0.5\%$ for $p_T^B \sim 10\,\text{GeV}$ to $\sim 19\%$ for $70 < p_T^B < 100\,\text{GeV}$, and from $\sim 4\%$ for $|y^B| \sim 0$ to $\sim 0.4\%$ for $1.8 < |y^B| < 2.4$.

The trigger and muon-reconstruction efficiencies are measured from a data sample of inclusive $J/\psi \to \mu^+\mu^-$ decays, using a technique similar to that described in Ref. [23], where one muon is identified with stringent quality requirements and the second muon is identified using information either exclusively from the tracker (to measure the trigger and muon-identification efficiencies) or from the muon system (to measure the silicon tracker efficiency). These measured efficiencies are compared to those resulting from the simulation studies, in bins of muon p_T and η, and seen to be in agreement within uncertainties. The measured and simulated efficiencies of the track reconstruction and of the vertex quality requirement are also found to

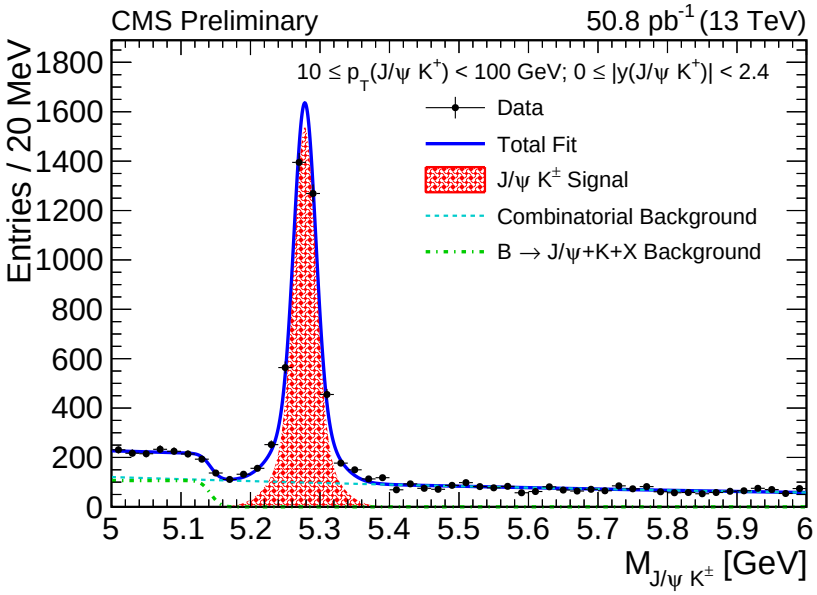

Figure 1: Invariant mass distribution of the $B^+ \to J/\psi K^+$ candidates, integrated in the phase space region $10 < p_T^B < 100\,\text{GeV}$ and $|y^B| < 2.4$. The solid curve shows the result of the fit. The shaded area represents the signal component, while the dashed and dash-dotted curves represent the combinatorial and mis-reconstructed $B \to J/\psi + K + X$ background components, respectively.

be compatible within their uncertainties. The residual difference between the measured and simulated efficiencies is taken as a systematic uncertainty.

5 Extraction of the signal yields

The signal yield is extracted with an extended unbinned maximum likelihood fit to the invariant mass distribution of the B^+ candidates, in each of the p_T^B or $|y^B|$ bins. The signal component is modeled by the sum of two Gaussians (representing the "core" and a "tail"). The relative normalization, mean, and width of the tail Gaussian are fixed with respect to those of the core Gaussian, following the shapes obtained from simulated samples. The combinatorial background component from the inclusive J/ψ production is described by an exponential function. The background from mis-reconstructed $B \to J/\psi + K + X$ decays is modeled by an error function. The relative normalization of the $B \to J/\psi + K + X$ component with respect to the signal is determined from a fit to all selected B^+ candidates, and is fixed in the fits to the candidates in each p_T^B or $|y^B|$ bin. The contribution from the CKM-suppressed decay $B^+ \to J/\psi\pi^+$ is found to be negligible; its effect is accounted for as a systematic uncertainty. Figure 1 shows the invariant mass distribution of all the B^+ candidates included in the analysis together with the corresponding fit result. The typical invariant mass distributions of the B^+ candidates, in one of the p_T^B bins and in one of the $|y^B|$ bins, are shown in Fig. 2.

6 Systematic uncertainties

The measured cross section is affected by systematic uncertainties on the extraction of the signal yields, efficiencies, branching fractions, and luminosity. The systematic uncertainties associated with the signal and background modeling are evaluated by changing the signal model

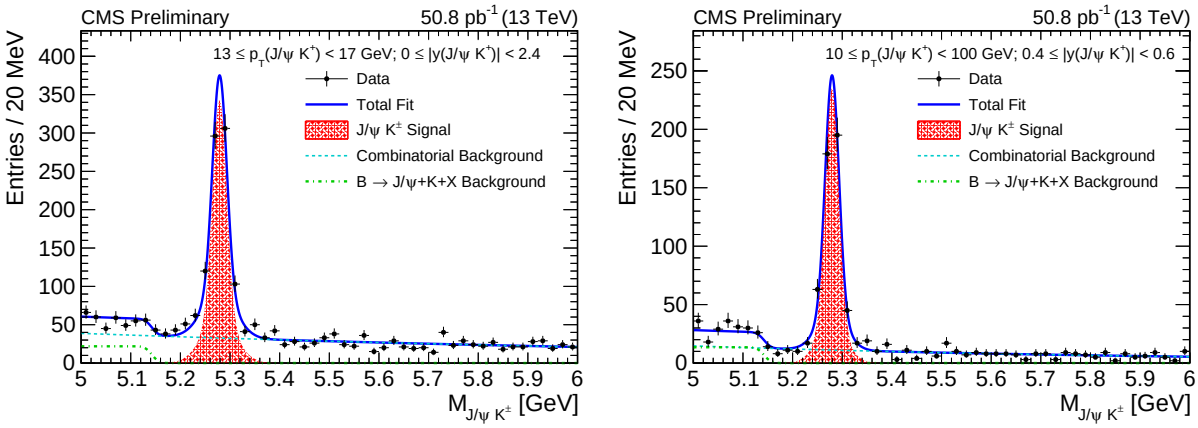

Figure 2: Invariant mass distributions of the $B^+ \to J/\psi K^+$ candidates in the regions of $13 \leq p_T^B < 17\,\text{GeV}$ (left) and $0.4 \leq |y^B| < 0.6$ (right). The solid curve shows the result of the fit. The shaded area represents the signal component, while the dashed and dash-dotted curves represent the combinatorial and mis-reconstructed $B \to J/\psi + K + X$ background components, respectively.

to the sum of three Gaussians and the combinatorial background model to a second order polynomial, respectively. The systematic uncertainty associated with the modeling of the mass distribution of mis-reconstructed $B \to J/\psi + K + X$ events is evaluated by comparing the error function to a Gaussian, and by shifting the error function by $\pm 10\,\text{MeV}$ in the mass dimension. The rare decay $B^+ \to J/\psi\pi^+$, neglected in the default analysis, is included in the fit for the purpose of evaluating a corresponding systematic uncertainty. Systematic uncertainties due to the finite resolution of the reconstructed p_T^B and y^B are determined by examining the generator information in the simulated samples. Half of the bin-to-bin migrated events are taken as the corresponding uncertainty. The uncertainties associated to the p_T^B and y^B distributions used in the generation of the simulated samples are evaluated with event-by-event weights determined from the differences between the distributions generated by PYTHIA and given by the FONLL calculations. The uncertainty on the B^+ lifetime is also included as a systematic uncertainty.

The events are triggered by a displaced J/ψ plus track combination; the uncertainty associated with the trigger criteria is evaluated by comparing the trigger efficiencies in data and in simulated samples, based on the events already triggered with a simpler inclusive J/ψ path. The difference between the trigger efficiencies in data and in simulated samples is included as a systematic uncertainty. The muon identification and reconstruction performances are also examined using a large sample of inclusive $J/\psi \to \mu^+\mu^-$ events, in data and in simulated events. The measured and simulated results are found to be consistent, and residual differences are considered as a systematic uncertainty. Furthermore, the uncertainty due to the limited sample size of simulated samples is also taken into account. A systematic uncertainty of 3.9% is taken for the charged track reconstruction. The luminosity has been measured with an uncertainty of 4.8%, while the uncertainty associated with the $B^+ \to J/\psi K^+ \to \mu^+\mu^- K^+$ branching fraction is 3.1%. The total uncertainties are evaluated as the sum in quadrature of the individual uncertainties.

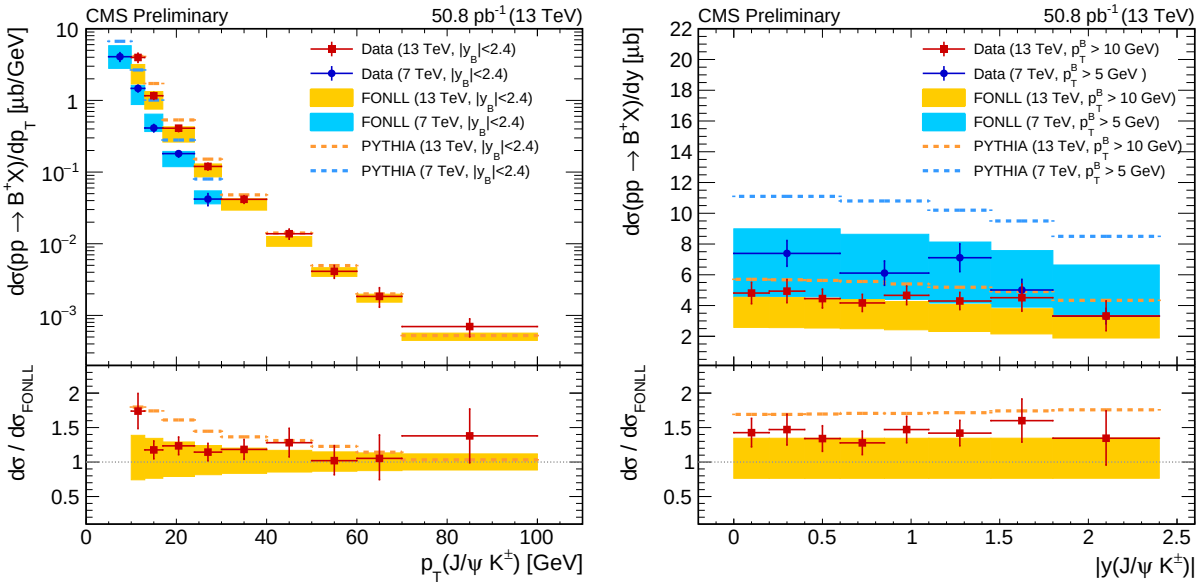

Figure 3: Differential cross sections $d\sigma/dp_{\mathrm{T}}^{\mathrm{B}}$ for $|y^{\mathrm{B}}| < 2.4$ (left) and $d\sigma/dy^{\mathrm{B}}$ for $10 < p_{\mathrm{T}}^{\mathrm{B}} < 100\,\mathrm{GeV}$ (right), for B^+ production in pp collisions at $\sqrt{s}$ =13 TeV. See the text for details.

7 Results

The differential cross sections for B^+ production as a function of $p_{\mathrm{T}}^{\mathrm{B}}$ for $|y^{\mathrm{B}}| < 2.4$, $d\sigma/dp_{\mathrm{T}}^{\mathrm{B}}$, and as a function of $|y^{\mathrm{B}}|$ (averaged for positive and negative rapidity) for $10 < p_{\mathrm{T}}^{\mathrm{B}} < 100\,\mathrm{GeV}$, $d\sigma/dy^{\mathrm{B}}$, are defined as

$$\frac{\mathrm{d}\sigma(\mathrm{pp}\to \mathrm{B}^+X)}{\mathrm{d}p_{\mathrm{T}}^{\mathrm{B}}} = \frac{n_{\mathrm{sig}}(p_{\mathrm{T}}^{\mathrm{B}})}{2\,A\cdot\epsilon(p_{\mathrm{T}}^{\mathrm{B}})\,\mathcal{B}\,\mathcal{L}\,\Delta p_{\mathrm{T}}^{\mathrm{B}}}\,, \qquad \frac{\mathrm{d}\sigma(\mathrm{pp}\to \mathrm{B}^+X)}{\mathrm{d}y^{\mathrm{B}}} = \frac{n_{\mathrm{sig}}(|y^{\mathrm{B}}|)}{2\,A\cdot\epsilon(|y^{\mathrm{B}}|)\,\mathcal{B}\,\mathcal{L}\,\Delta y^{\mathrm{B}}}\,, \quad (1)$$

where $n_{\mathrm{sig}}(p_{\mathrm{T}}^{\mathrm{B}})$ and $n_{\mathrm{sig}}(|y^{B}|)$ are the fitted signal yields in the $p_{\mathrm{T}}^{\mathrm{B}}$ or $|y^{B}|$ bins, respectively; $\Delta p_{\mathrm{T}}^{\mathrm{B}}$ and $\Delta y^{\mathrm{B}} = 2\Delta|y^{\mathrm{B}}|$ are the bin widths. The branching fraction $\mathcal{B}$ is the product of the individual branching fractions $\mathcal{B}(\mathrm{B}^+ \to \mathrm{J}/\psi\mathrm{K}^+) = (1.026 \pm 0.031) \times 10^{-3}$ and $\mathcal{B}(\mathrm{J}/\psi \to \mu^+\mu^-) = (5.961 \pm 0.033) \times 10^{-2}$ [19]. The factor of two in the denominator reflects the choice to quote the cross section for a single charge (taken to be the B^+), while n_{sig} includes both charge states. The efficiency times acceptance, $A\cdot\epsilon(p_{\mathrm{T}}^{\mathrm{B}})$ and $A\cdot\epsilon(|y^{\mathrm{B}}|)$, is calculated for each bin, and accounts for bin-to-bin migrations (up to a few percent) due to the resolution of the measured momentum and rapidity.

The differential cross sections as a function of $p_{\mathrm{T}}^{\mathrm{B}}$, integrated within $|y^{B}| < 2.4$, and as a function of y^{B}, integrated within $10 < p_{\mathrm{T}}^{\mathrm{B}} < 100\,\mathrm{GeV}$, are shown in Fig. 3 (left and right panels, respectively), where they are compared to FONLL (shaded boxes) and PYTHIA (dashed lines) calculations. The 7 TeV measurements are also displayed, for completeness. The bottom panels display the data over FONLL cross section ratios; the PYTHIA/FONLL ratios are also shown, as dashed lines.

8 Summary

In summary, the differential cross section for B^+ production in pp collisions at $\sqrt{s}$ =13 TeV has been measured using the decay channel $\mathrm{B}^+ \to \mathrm{J}/\psi\mathrm{K}^+$, with $\mathrm{J}/\psi \to \mu^+\mu^-$, as a function of $p_{\mathrm{T}}^{\mathrm{B}}$

for $|y^{\mathrm{B}}| < 2.4$ and as a function of y^{B} for $10 < p_{\mathrm{T}}^{\mathrm{B}} < 100\,\mathrm{GeV}$. The measured values show a reasonable agreement, both in terms of shape and of normalization, with FONNL calculations and with the results obtained with the PYTHIA event generator.

References

[1] UA1 Collaboration, "Beauty production at the CERN proton - anti-proton collider", *Phys. Lett.* **B186** (1987) 237, doi:10.1016/0370-2693(87)90287-5.

[2] UA1 Collaboration, "Measurement of the bottom quark production cross section in proton-anti-proton Collisions at $\sqrt{s} = 0.63\,\mathrm{TeV}$", *Phys. Lett.* **B213** (1988) 405, doi:10.1016/0370-2693(88)91785-6.

[3] CDF Collaboration, "Measurement of the B meson differential cross-section, $d\sigma/dp_{\mathrm{T}}$, in $p\overline{p}$ collisions at $\sqrt{s} = 1.8\,\mathrm{TeV}$", *Phys. Rev. Lett.* **75** (1995) 1451, doi:10.1103/PhysRevLett.75.1451.

[4] CDF Collaboration, "Measurement of the B^+ total cross section and B^+ differential cross section $d\sigma/dp_T$ in $p\overline{p}$ collisions at $\sqrt{s} = 1.8\,\mathrm{TeV}$", *Phys. Rev.* **D65** (2002) 052005, doi:10.1103/PhysRevD.65.052005.

[5] CDF Collaboration, "Measurement of the J/ψ meson and b-hadron production cross sections in $p\overline{p}$ collisions at $\sqrt{s} = 1960\,\mathrm{GeV}$", *Phys. Rev.* **D71** (2005) 032001, doi:10.1103/PhysRevD.71.032001.

[6] CDF Collaboration, "Measurement of the B^+ production cross section in $p\overline{p}$ collisions at $\sqrt{s} = 1960\,\mathrm{GeV}$", *Phys. Rev.* **D75** (2007) 012010, doi:10.1103/PhysRevD.75.012010.

[7] D0 Collaboration, "Inclusive μ and b quark production cross-sections in $p\overline{p}$ collisions at $\sqrt{s} = 1.8\,\mathrm{TeV}$", *Phys. Rev. Lett.* **74** (1995) 3548–3552, doi:10.1103/PhysRevLett.74.3548.

[8] D0 Collaboration, "Cross section for b jet production in $\overline{p}p$ collisions at $\sqrt{s} = 1.8\,\mathrm{TeV}$", *Phys. Rev. Lett.* **85** (2000) 5068–5073, doi:10.1103/PhysRevLett.85.5068.

[9] CMS Collaboration, "Measurement of the B^+ production cross section in pp collisions at $\sqrt{s} = 7\,\mathrm{TeV}$", *Phys. Rev. Lett.* **106** (2011) 112001, doi:10.1103/PhysRevLett.106.112001, arXiv:1101.0131.

[10] CMS Collaboration, "Inclusive b-hadron production cross section with muons in pp collisions at $\sqrt{s} = 7\,\mathrm{TeV}$", *JHEP* **03** (2011) 090, doi:10.1007/JHEP03(2011)090, arXiv:1101.3512.

[11] CMS Collaboration, "Measurement of the B^0 production cross section in pp collisions at $\sqrt{s} = 7\,\mathrm{TeV}$", *Phys. Rev. Lett.* **106** (2011) 252001, doi:10.1103/PhysRevLett.106.252001, arXiv:1104.2892.

[12] CMS Collaboration, "Measurement of the strange B meson production cross section with J/$\psi\phi$ decays in pp collisions at $\sqrt{s} = 7\,\mathrm{TeV}$", *Phys. Rev.* **D84** (2011) 052008, doi:10.1103/PhysRevD.84.052008, arXiv:1106.4048.

[13] ATLAS Collaboration, "Measurement of the b-hadron production cross section using decays to $D^*\mu^- X$ final states in pp collisions at $\sqrt{s} = 7\,\mathrm{TeV}$ with the ATLAS detector",

Nucl. Phys. **B864** (2012) 341, doi:10.1016/j.nuclphysb.2012.07.009, arXiv:1206.3122.

[14] ATLAS Collaboration, "Measurement of the differential cross-section of B^+ meson production in pp collisions at $\sqrt{s}$ = 7 TeV at ATLAS", *JHEP* **10** (2013) 042, doi:10.1007/JHEP10(2013)042, arXiv:1307.0126.

[15] LHCb Collaboration, "Measurement of the $B^\pm$ production cross-section in pp collisions at $\sqrt{s} = 7$ TeV", *JHEP* **04** (2012) 093, doi:10.1007/JHEP04(2012)093, arXiv:1202.4812.

[16] LHCb Collaboration, "Measurement of B meson production cross-sections in proton-proton collisions at $\sqrt{s}$ = 7 TeV", *JHEP* **08** (2013) 117, doi:10.1007/JHEP08(2013)117, arXiv:1306.3663.

[17] LHCb Collaboration, "Measurement of B_c^+ production in proton-proton collisions at $\sqrt{s} = 8$ TeV", *Phys. Rev. Lett.* **114** (2015), no. 13, 132001, doi:10.1103/PhysRevLett.114.132001, arXiv:1411.2943.

[18] CMS Collaboration, "The CMS experiment at the CERN LHC", *JINST* **3** (2008) S08004, doi:10.1088/1748-0221/3/08/S08004.

[19] K. A. Olive and others (Particle Data Group), "Review of Particle Physics", *Chin. Phys.* **C38** (2014) 090001 and 2015 update, doi:10.1088/1674-1137/38/9/090001.

[20] T. Sjostrand, S. Mrenna, and P. Z. Skands, "A brief introduction to PYTHIA 8.1", *Comput. Phys. Commun.* **178** (2008) 852, doi:10.1016/j.cpc.2008.01.036, arXiv:0710.3820.

[21] "The EVTGEN particle decay simulation package", *Nucl. Instrum. Meth.* **A462** (2001) 152, doi:doi:10.1016/S0168-9002(01)00089-4.

[22] GEANT4 Collaboration, "GEANT4: A simulation toolkit", *Nucl. Instrum. Meth.* **A506** (2003) 250–303, doi:doi:10.1016/S0168-9002(03)01368-8.

[23] CMS Collaboration, "Prompt and non-prompt J/ψ production in pp collisions at $\sqrt{s} = 7$ TeV", *Eur. Phys. J.* **C71** (2011) 1575, doi:10.1140/epjc/s10052-011-1575-8, arXiv:1011.4193.